Solvent Effects on IR and VCD Spectra of Helical Peptides: DFT-Based Static Spectral Simulations with Explicit Water

ARTICLE *in* THE JOURNAL OF PHYSICAL CHEMISTRY B · MAY 2005

Impact Factor: 3.3 · DOI: 10.1021/jp0506078 · Source: PubMed

Solvent Effects on IR and VCD Spectra of Helical Peptides: DFT-Based Static Spectral Simulations with Explicit Water

Jan Kubelka,† Rong Huang, and Timothy A. Keiderling*

Department of Chemistry (M/C 111), University of Illinois at Chicago, 845 W. Taylor Street, room 4500 SES, Chicago, Illinois 60607-7061

Received: February 3, 2005

Simulations of IR and VCD spectra are carried out for model α-helical, 3_{10}-helical, and 3_1-helical (polyProII-like) oligopeptides, with up to 21 amide groups, and including explicit consideration of effects of directly hydrogen-bonded solvent (water). Parameters used were obtained from ab initio density functional theory (DFT) computations of force field, atomic polar and axial tensors for oligopeptides of 5 to 7 amides, whose structures were constrained in (ϕ,ψ) to target the secondary structure type but otherwise fully optimized. By comparison with experimental data as well as with calculations for identical but isolated (gas phase) peptides, the computed effects of an inner shell of aqueous solvent on the vibrational spectra of helical oligopeptides are illustrated. The interaction with solvent causes significant frequency shifts of the amide bands, but only minor changes in the characteristic IR intensity distributions and splittings and the VCD band shapes. Better agreement with experimental band shapes is achieved for the α-helical amide I′ (N-deuterated) VCD by inclusion of explicit solvent in the calculations. Some improvements are also observed in theoretical VCD predictions for ^{13}C labeled α-helical peptides when solvated models are used. However, the qualitative isotopic splitting patterns are preserved and just shifted in frequency due to consistent, solvent independent interamide coupling constants. The critical match of experiment and theory for relative positions of transitions in peptides with specifically separated ^{13}C═O labels, including and neglecting solvent, confirms the stability of the coupling interactions. Despite these solvation effects, the calculated VCD band shape of the amide I mode is shown to be a reliable conformational probe, since it remains basically insensitive to frequency shifts caused by environment. Thus theoretical VCD simulations, even vacuum calculations, are shown to provide useful spectral predictions for solution-phase peptides.

Introduction

Infrared absorption (IR) and vibrational circular dichroism (VCD) spectroscopies (as well as their Raman counterparts) have proven their potential for conformational analyses of peptides and proteins.[1,2] However, their inherently low resolution often makes analysis of vibrational spectra in terms of conformation difficult. Most traditional approaches to structural interpretation of proteinic vibrational spectra are based on empirical correlations of structural type and vibrational frequencies (for IR and also Raman) or spectral band shapes (for VCD) using as standards spectra of polypeptides that adopt unique conformations or, alternatively, proteins with known structure. Unfortunately, IR frequency assignments to particular secondary structural types have been shown to be non-unique.[3−5] One of the reasons is that, even for a given structural type, the vibrational frequencies vary due to nonstructural perturbations, among which interaction with solvent stands out. It has been shown that the amide I (primarily amide C═O stretch), which is most commonly used for determination of secondary structure by IR spectroscopy, can exhibit large frequency shifts depending on the solvent environment.[6−9] On the other hand, VCD band shapes are known to be largely immune to solvent-induced frequency shifts and thus have a potential to provide more reliable structural information than vibrational frequencies.[2,10]

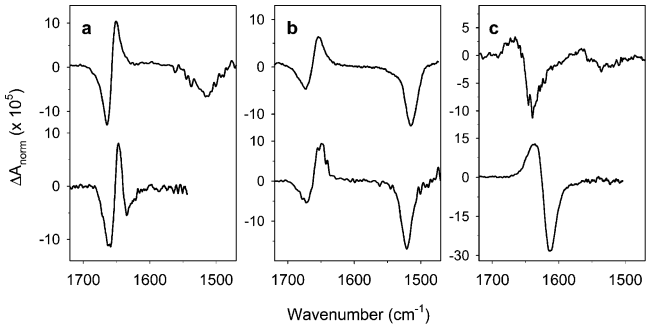

Figure 1. Examples of VCD spectra for different secondary structures. (a) α-helix; top: $(Met_2Leu)_6$ (amide I and II, nonaqueous), bottom; Ac−$(Ala_4Lys)_4$−(Ala_4Tyr)−ND_2 (amide I′ in D_2O). (b) 3_{10}-helix; top: $(\alpha\text{-Me-Val})_8$; bottom: Aib_5−Leu−Aib_2 (both nonaqueous). (c) top: "random coil" poly(Lys) (in H_2O), bottom: polyProII-helix $(Pro)_{12}$ (in D_2O). All amino acid residues except Aib are L-configuration.

Characteristic amide I (amide I′ in D_2O) and amide II VCD spectra for the basic helical oligopeptide secondary structures are shown in Figure 1.

Theoretical simulations of the spectra for the model peptide structures in question can provide more rigorous approaches to spectral interpretation. Accurate simulation of VCD requires quantum mechanical level calculations, which would be prohibitively large for macromolecules such as proteins and even prove difficult for most oligopeptides large enough to adopt a stable secondary structure in solution. However, as we have

* To whom correspondence should be addressed. E-mail: tak@uic.edu.
† Present address: Laboratory for Chemical Physics, NIDDK, National Institutes of Health, Bethesda, MD 20892-0520.

10.1021/jp0506078 CCC: $30.25
Published on Web 03/30/2005

demonstrated, density functional theory (DFT) level calculations of vibrational frequency (i.e., force-field, FF) and intensity (atomic polar and axial tensors, APT and AAT) parameters for small, conformationally constrained peptides yield spectral predictions in qualitative agreement with experiment for several secondary structural types.[11−20] When such DFT-generated parameters are transferred onto larger structures using our property tensor method,[21] we can obtain simulated vibrational spectra for sizable oligopeptides and protein fragments for which local interactions are computed to a DFT level. We have applied this methodology to detailed studies of IR and VCD spectral features for helical[11−13,16,17] as well as β-sheet[14,15,18,19] models and have shown that this approach using transferred DFT parameters can yield valuable insights into spectral effects caused by, for example, ^{13}C isotopic substitutions,[11−13] $C^{\alpha\alpha}$-dimethylated amino acids,[16,22] and proline residues.[19] Thus far, most of our spectral simulations were carried out for isolated peptides that formally correspond to the gas phase (vacuum). Amide vibrational mode frequencies calculated for peptides in the gas phase are systematically in error (typically high) when compared to experiments carried out in aqueous solution. However, the mode dispersion and ordering, which is reflected in the IR by the splitting and intensities of the amide originating bands, and in the VCD by their sign and shape, are generally in good qualitative agreement with experiment. Therefore, these properties manifest interactions characteristic of the peptide backbone conformation that are less sensitive to other effects such as solvent and sidechains.

Peptide−water interactions have very large effects on the amide vibrational frequencies causing frequency shifts as large as 100 cm^{-1} in the amide I.[6,8,9] Such large shifts might suggest that the amide VCD could also be affected by solvent, since the interactions giving rise to the relative ordering of normal modes within the amide I are on the order of just a few cm^{-1}. For these reasons, explicit modeling of solvent effects on the vibrational spectra of amino acids as well as small amides has been the subject of several previous studies.[23−27] Unfortunately, such small molecules have only limited applicability for analyses of vibrational spectra for larger oligopeptides or proteins. Rather, theoretical analyses of solvent effects on vibrational spectra of oligopeptides that model protein secondary structures are necessary for interpreting spectroscopic data used in protein conformational studies, including protein folding and enzymatic mechanisms.

For helical oligopeptides, the experimental evidence as well as our success in modeling experimental spectra using gas phase calculations suggest that there are only modest solvent effects on the VCD, despite the large overall frequency shift. Our preliminary simulation results for a solvated β-turn peptide[19] and of an α-helical triamide fragment[13] thus far are consistent with these observations. However, some detailed qualitative features and quantitative intensity patterns experimentally measured in solution are not fully predicted by the gas-phase calculations. Examples where improved simulations are needed for helical peptides include the negative−positive−negative (−,+,−) amide I VCD of N-deuterated (in D_2O) α-helices[10] and the enhanced VCD of the ^{13}C amide I side band for isotopically labeled α-helical peptides.[12]

In this report, we present simulations of vibrational spectra (IR and VCD) for explicitly solvated peptides of up to 20 residues in α-, 3_{10}- and 3_1-(poly-proline II-like) helical conformations. The computing power available to us allowed DFT calculations to be carried out for solvated peptide fragments (here meaning the inner shell of water, making the amides fully H-bonded) that were large enough to include most of the important intrahelical interactions. For realistic comparison with experimental data, these parameters are used to simulate the spectra of much larger peptide helices, constructed to mimic molecules that have been experimentally studied. The predicted effects of solvent on spectral characteristics are analyzed by comparison of the simulated spectra for identical peptides in vacuum and with explicit solvent. We have also applied these parameters to spectral simulations for several ^{13}C-labeled helical oligopeptides to gain an insight into the dependence of IR and VCD intensity patterns on label positions and to evaluate the effect of solvent on vibrational coupling of specifically labeled amides.

TABLE 1: Notation, Sequences, and Conformational Parameters for Model Peptides

notation	sequence[a]	secondary structure	dihedral angle [deg] ϕ	ψ	ω
A7 (A7W)	Ac−A_6−NH−CH_3	α-helix	−57	−47	180
A21 (A21W)	Ac−A_{20}−NH−CH_3				
T5 (T5W)	Ac−A_4−NH−CH_3	3_{10}-helix	−60	−30	180
T21 (T21W)	Ac−A_{20}−NH−CH_3				
P5 (P5W)	Ac−A_4−NH−CH_3	3_1-helix	−78	+149	180
P21 (P21W)	Ac−A_{20}−NH−CH_3	(polyPro II-like)			

[a] A represents L-Ala, Ac is acetyl N-terminus blocking group, NH−CH_3 is an amino C-terminus blocking group, both of which create an amide bond that couples to the peptide sequence.

Methods

Model Structures. All peptide models in this study are based on L-alanine (Ala), the smallest amino acid that contains a chiral α-carbon. The initial starting structures for the optimization of α-helical, 3_{10}-helical, and 3_1-helical (left-handed, polyProII-like) peptides were constructed using standard conformational parameters,[28] summarized in Table 1. The α-helical hepta-amide Ac−Ala_6−NH−CH_3 (denoted **A7**) and 3_{10}-helical penta-amide Ac−Ala_4−NH−CH_3 (**T5**) were used as minimal models for these helical types. In these models the central amide is hydrogen bonded both back and forward in the sequence on its carbonyl and amino groups, respectively. This ensures that the model has representation of all types of residues in the helix, central (fully internally hydrogen bonded) and terminal (partially hydrogen-bonded from either N− or C− terminus).[12,13] The left-handed 3_1-helix (polyProII-like, also denoted 3_2-helix) does not form intramolecular hydrogen bonds, and a penta-amide (**P5**) was selected as its basic model.

To simulate the effects of the solvent, water molecules were added to the minimal internally hydrogen bonded α- and 3_{10}-helical model peptides, **A7**, **T5**, as well as to the 3_1-helical **P5**, to represent the first hydration layer, i.e., waters directly interacting with the peptide via hydrogen bonds. These peptide−water complexes **A7W**, **T5W**, and **P5W** were constructed assuming two hydrogen-bonding sites were possible on the carbonyl oxygen and one on the amino group. In the α- and 3_{10}-helical models, two water molecules were added to each amide C═O and one to each amide N−H group that do not participate in the intrahelical hydrogen bonding. Likewise, in the 3_1-helical model, where no intrapeptide hydrogen bonds are present, two water molecules were hydrogen bonded to each oxygen and one to each amino group. The initial geometries for the H_2O-amide bonds in these groups, before optimization, were derived from the hydrogen bonded *N*-methyl acetamide (NMA) complex with three H_2O molecules.[23,29−33] For the amide carbonyl groups that have single intrahelical hydrogen bond,

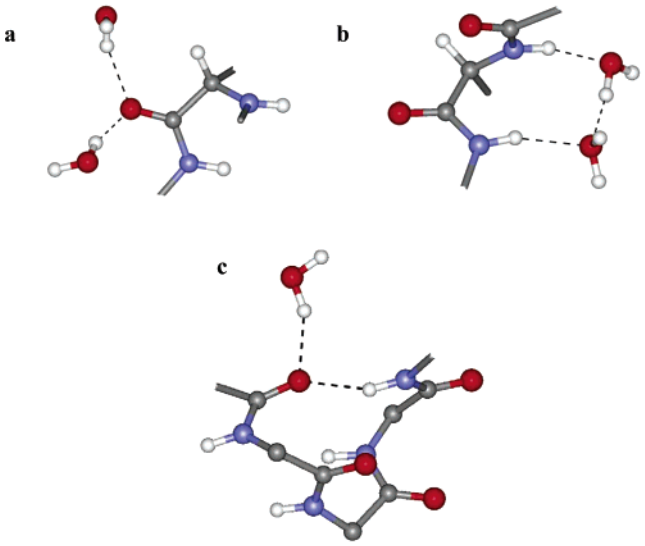

Figure 2. Hydrogen bonding of water to the amide groups in the α-helical peptide: (a) noninternally hydrogen-bonded C═O at the C-terminus, (b) noninternally hydrogen-bonded N−H at the N-terminus, (c) internally hydrogen-bonded C═O in the continuing helix.

the starting configuration of the added water was based on X-ray structures of hydrated protein segments.[34] The α-helical **A7W** structure for the terminal and central amides is illustrated in Figure 2. This procedure resulted in 13 hydrogen bonded water molecules for the **A7W** α-helical structure, 9 hydrogen bonded water molecules for the **T5W** 3_{10}-helical structure, and 15 water molecules for the **P5W** 3_1-helix. Prior to the DFT optimization and vibrational calculations, the solvent configuration in the peptide−water complexes was first pre-optimized by molecular mechanics (MM) energy minimization. The AMBER force field,[35] was used for this purpose and the MM energy minimization was carried out with the Discover module of the Insight II program package.[36]

Alanine 20-mers, Ac−(L-Ala)$_{20}$−NH−CH$_3$, containing 21 amide bonds were used as full-size models for previously experimentally studied α-helical peptides of the same length.[12] The 20-mer oligopeptides were again based on repeating units with the standard, idealized α-helical (**A21**), 3_{10}-helical (**T21**), and 3_1-helical (**P21**) torsional (ϕ,ψ) angles (Table 1). Local geometrical parameters (bond lengths and angles) in these models were in fact DFT-optimized since they were constructed from DFT energy-minimized (as described below) short oligopeptide structures (**A7**, **T5**, and **P5**).

Two separate tests of isotopically labeled variants of the α-helical **A21** and 3_1-helical **P21** theoretical models were undertaken. The first group each had four sequential residues amide ^{13}C═O labeled, whose placement was chosen to correspond to a set of experimentally studied isotopomers of the Ala-rich 20-mer peptide, listed in Table 2. To keep the notation simple and consistent with that used for the experimental models (see below), the different (vacuum) molecule models will be denoted **U21** for the unlabeled (equivalent to A21 for α-helical), **N21** for the N-terminally labeled peptide, **M21** for middle labeled, and **C21** for C-terminally labeled oligomers. Likewise, the solvated isotopomers (derived from **A21W**) will be abbreviated as **U21W**, **N21W**, etc.

The second group of isotopically labeled peptides had two ^{13}C labeled residues (on the amide C═O), placed roughly in the center of the sequence, but with variable spacing. For these isotopic variants the notation used in our previous study of vibrational couplings in these peptides[20] is followed: **2LT** for adjacent isotopically labeled residues, and **2LnS** (n=1, 2 or 3) for the labeled residues separated by n=1, 2, or 3 unlabeled ones. Similar comparative computations were carried out for 3_{10}- and 3_1-helices.

DFT Calculations. All quantum mechanical calculations were carried out at the DFT level, using the Gaussian 98 program package.[37] The BPW91 density functional[38,39] with a 6-31G* basis set[40] was used in all cases. The geometries of all the models, **A7**, **T5**, and **P5**, including those with explicit water molecules **A7W**, **T5W**, and **P5W**, were fully optimized with the exception that just the ϕ, ψ, ω torsional angles were constrained to yield the target helical conformations. In particular, this method results in the water hydrogen-bond geometries finding one local minimum. The geometry was considered optimized when all the default convergence criteria of Gaussian 98[41] were met.

For the optimized structures, analytical harmonic FF and analytical APT and AAT were calculated at the same level of theory. The AAT in Gaussian 98 are implemented according to the magnetic field perturbation (MFP) theory of Stephens[42] with gauge-including atomic orbitals (GIAO).[43] Isolated peptide calculations were carried out on the UIC HP 9000/800 computer, using four CPUs. The calculations for the peptide−water complexes were carried out using four CPUs on a Beowulf type PC cluster (Paralogic, Inc., Bethlehem, PA) in the UIC Department of Chemistry, through the kind provision of Prof. Cynthia Jameson and Dr. Devin Sears.

Transfer of the Property Tensors. Vibrational FF and associated APT and AAT intensity parameters for large, isolated oligopeptides **A21**, **T21**, and **P21** were obtained by transfer of the Cartesian FF, APT, and AAT matrices calculated at the DFT level for the respective isolated small peptides (**A7**, **T5**, and

TABLE 2: Notation and Sequences for ^{13}C Isotopically Labeled α-helical Peptides

notation	label position	sequence[a]
		Experimental Models
U	unlabeled	Ac-AAAAKAAAAKAAAAKAAAAY−NH$_2$
N	N-terminus	Ac-A*A*A*A*KAAAAKAAAAKAAAAY−NH$_2$
M	middle	Ac-AAAAKA*A*A*A*KAAAAKAAAAY−NH$_2$
C	C-terminus	Ac-AAAAKAAAAKAAAAKA*A*A*A*Y−NH$_2$
		Theoretical Models
U21 (U21W)	unlabeled	Ac−AAAAAAAAAAAAAAAAAAAA−NH−CH$_3$
N21 (N21W)	N-terminus	Ac−A*A*A*A*AAAAAAAAAAAAAAAA−NH−CH$_3$
M21 (M21W)	middle	Ac−AAAAAA*A*A*A*AAAAAAAAAA−NH−CH$_3$
C21 (C21W)	C-terminus	Ac−AAAAAAAAAAAAAAAA*A*A*A*A−NH−CH$_3$
2LT	middle	Ac−AAAAAAAAAAA*A*AAAAAAA−NH−CH$_3$
2L1S	middle	Ac−AAAAAAAAAA*AA*AAAAAAA−NH−CH$_3$
2L2S	middle	Ac−AAAAAAAAAA*AAA*AAAAAA−NH−CH$_3$
2L3S	middle	Ac−AAAAAAAAA*AAAA*AAAAAA−NH−CH$_3$

[a] The ^{13}C (on C═O) labeled residues are indicated by " * ". A = L-Ala, K = L-Lys.

P5). The procedure used for transfer of Cartesian tensors is decribed in detail elsewhere.[21] In brief, the short peptide fragment for which the FF, APT, and AAT are determined from the DFT calculation is sequentially overlapped, amide by amide group, with all large oligomer segments of the same length. For each such overlap, the smaller structure is first rotated to the same orientation, the rotation matrices are used to transform the Cartesian FF, APT, and AAT matrices to the correct coordinate system of the particular large peptide segment, and these transformed FF, APT, and AAT are transferred to the corresponding atoms of the segment. The sequential overlap between segments ensures that proper vibrational coupling for each amide linkage is included in the transferred FF.

To eliminate interference of the water molecule vibrations, the DFT-computed FF, APT, and AAT parameters from the oligopeptide−water complexes **A7W**, **T5W**, and **P5W** were transferred to the identical oligopeptides, but without the water molecules. In this way the peptides FF, APT, and AAT all contain the interactions with solvent, but the solvent itself is deleted from the vibrational spectra. Eliminating the explicit water while keeping the interactions only simplifies the computed spectra and thus aids the comparison between isolated and solvated peptide spectral simulations as well as between simulated and experimental spectra. This partially mimics the standard method of subtraction of solvent water absorbance from the experimental peptide IR spectra. The impact is most dramatic for the amide I mode which overlaps the H−O−H deformation, now eliminated from the simulations. We have previously carried out several tests of the ability of the transfer method to faithfully replicate the DFT results for modest sized oligomers where the spectral band shapes for transferred and fully DFT calculated spectra were functionally identical.[13,15,44] This approach for eliminating the solvent interference from peptide−water simulations was subject to further testing and its validity will be demonstrated in the Discussion section. In a similar way the FF, APT, and AAT from explicitly solvated small helical segments **A7W**, **T5W**, and **P5W** were transferred onto the corresponding large oligomers **A21**, **T21**, and **P21**. Although these oligopeptides in fact do not contain any explicit solvent molecules, again, the solvent interactions are present in the transferred parameters and thus its simulated spectra correspond to the solvated molecule and are denoted **A21W**, **T21W**, and **P21W**.

Simulation of the Spectra. Simulation of the IR absorption and VCD spectra using molecular coordinates and associated FF, APT, and AAT values, extracted from the Gaussian 98 or the parameter transfer program output, were performed using a set of programs originally written by Petr Bour, Czech Academy of Science, and extended in-house.[13,21] The FF was first corrected for translations and rotations, mass weighted, and diagonalized. The normal mode eigenvectors (S-matrices) were contracted with the APT and AAT parameters to produce the resulting dipole (D) and rotational (R) strengths. The final spectral band shapes for IR or VCD simulations were obtained by summing over normal modes each represented by a Lorentzian function with a full width at half-maximum (fwhm) of 20 cm^{-1}, and area proportional to D or R, respectively. The programs for vibrational analysis also permit isotopic substitutions. Since isotopic substitution in the harmonic approximation does not affect either the FF or APT and AAT, it is implemented by simply changing the masses of atoms to be substituted, such as D_2O for H_2O, amide N-deuteration, or ^{13}C on amide C═Os. In addition, to remove the computed vibrational overlap and interference from the $-CH_3$ groups in the amide II region, deuterium was substituted for methyl hydrogens.[11,13,37] Such side chains pose no real spectral interference, since the experimental frequency separation between $-CH_3$ and amide II vibrations is larger than calculated and their coupling is relatively weak. Thus computational "removal" is the best way to mimic experiment.

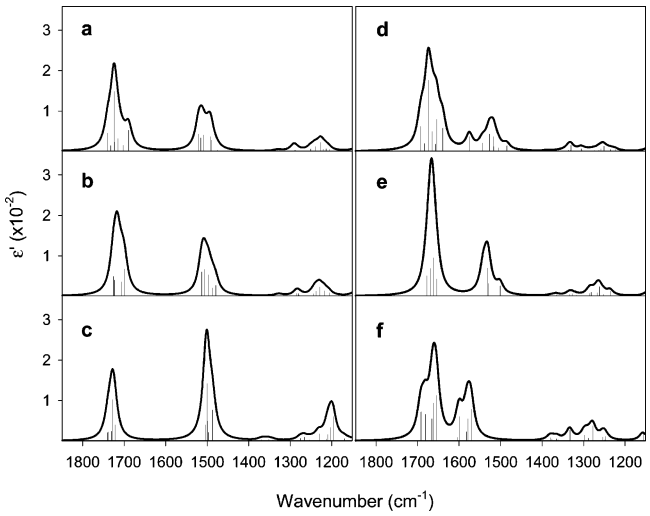

Figure 3. Fully DFT simulated IR spectra for the isolated and solvent-modified shorter model peptides. Isolated peptides (left): (a) α-helical **A7**, (b) 3_{10}-helical **T5**, and (c) 3_1-helical **P5**. Solvated peptides (right): (d) α-helical **A7W**, (e) 3_{10}-helical **T5W**, and (f) 3_1-helical **P5W**. Intensity of the band envelope is molar extinction coefficient per amide group. Vertical lines indicate position and dipole strength of component bands.

Comparison Data. Computational results for ^{13}C isotopically labeled models are compared to previously published experimental IR and VCD spectra measured in our laboratory for a series of ^{13}C labeled alanine-rich peptides (sequences and notation in Table 2) that are predominantly helical at low temperatures.[12,20]

Results

DFT-Level Simulations of Spectra for Small Helical Oligopeptides. Comparisons of the DFT simulated IR spectra for isolated and solvated (**-W**) α- (**A7, A7W**), 3_{10}- (**T5, T5W**), and 3_1- (**P5**, **P5W**) helical segments are shown in Figure 3. The isolated peptide spectra are characterized by the amide I band computed to be around 1720 cm^{-1} and the amide II near 1510 cm^{-1}, a separation which is nearly 100 cm^{-1} more than seen experimentally for the amide I−II differences in such helices in solution (see Figure 1). The 3_{10}-helix is predicted to have somewhat lower amide I vibrational frequency than the α-helix maximum and the 3_1-helix somewhat higher, both not what is normally observed. Both α- and 3_{10}-helical amide I bands show a low frequency shoulder (mostly due to the N-terminal amide), with more dispersion for the α-helix component transitions. The 3_1-helix shows much less dispersion between the components of particular amide modes and, in vacuum, has a more intense amide II than amide I, again in contrast to most experimental solution observations.

The most obvious effect of hydrogen bonding to the water solvent is a change in the (diagonal) force field resulting in a significant shift in computed amide vibrational frequencies. In particular, the amide I envelope shifts lower by >50 cm^{-1} and the amide II, on the other hand, shifts higher but to a lesser extent (except for **P5W**). In addition, for the solvated models the IR amide I bands are predicted to be more intense and the amide II less intense than in vacuum. The amide I for the

α-helical **A7W** peptide appears at ∼1670 cm^{-1}, which though still too high compared to experimental values for fully solvated α-helical oligopeptides in aqueous solution (1630−40 cm^{-1}), and even compared to protein (partially hydrated) values (∼1650 cm^{-1}), are much closer to experiment than are the isolated molecule calculations. The predicted α-helical amide II has several components, the resolved one at 1575 cm^{-1} is localized on the N-terminal amide group with the remainder clustered around the ∼1521 cm^{-1} maximum.

The amide I and II maxima for the solvated 3_{10}-helix (**T5W**) are predicted at ∼1666 and 1533 cm^{-1}, respectively. As for the vacuum simulations, mode dispersion is reduced for the 3_{10}-helix, much less for the amide II, and fewer changes from vacuum are seen, compared to the α-helix (compare Figure 3d and 3e). The mode dispersions reflect substantial "end-effects" in these short oligopeptide models, where more residues constitute termini than those in continuing, repetitive structures of higher oligomers.

The largest frequency shifts upon solvation are predicted for the 3_1-helix, where both the amide I and amide II shift by ∼70 cm^{-1} but in opposite directions so their splitting becomes <100 cm^{-1}. In comparison to what is seen for the other helices, this differentially large amide I−II contraction on adding waters is most likely artificial in that each amide group changes from no hydrogen bonds in **P5** to three for **P5W** (two on C═O, one on N−H) due to the absence of intrahelical hydrogen bonds, while the **A7** and **T5** structures are already partially H-bonded. The **P5W** amide I (∼1660 cm^{-1}) is still predicted higher than observed experimentally (∼1640 cm^{-1} for "random coil" poly-(L-Lys)). The 3_1-helix amide II frequency (∼1580 cm^{-1}) is also predicted higher than seen experimentally (1550 cm^{-1}), making the calculated amide I−II splitting reasonable. This is in contrast to results for the other two hydrated helices, as well as for all isolated molecule calculations, where the calculated amide II is lower in frequency than the experimental value. While for the isolated **P5** the computed amide II IR intensity is greater than that of the amide I, in sharp contrast to experiment, this ratio is reversed to an experimentally reasonable relationship for the solvated **P5W**.[11,13,17] These comparisons to experiment are complicated because "random coil" polypeptides are only locally 3_1-helical, presumably maintaining a large degree of disorder, while polyPro-II, which does form extended, highly ordered 3_1-helices, has no amide II mode since, due to having tertiary amide links, Pro peptides lack an N−H.

The corresponding DFT VCD spectra for the same isolated and solvated helical segments are compared in Figure 4. In vacuum, the amide I VCD for all three peptide conformations reflects the characteristic shapes observed experimentally (Figure 1), that is an intense positive couplet (positive followed by negative with increasing wavenumber) for the α-helix, a weaker positive couplet for the 3_{10}-helix, and an intense negative couplet for the 3_1-helix. Likewise, amide II VCD band shapes, weak and broad for the α-helix but narrower and more intense for the 3_{10}-helix, are in good correspondence with experimental observations (Figure 1).[45−47] The negative extremum of the α-helical amide II VCD, however, is often observed lower in frequency than the corresponding absorption maximum, while in the simulation it appears more in alignment. The amide II in the 3_1-helix in vacuum yields a weak negative band, although a broad negative couplet shape has been seen experimentally (Figure 1). The amide III modes are highly dispersed and mixed with the C_α−H deformations. Although for all conformations the sum over the components (1200−1400 cm^{-1}) is net positive,

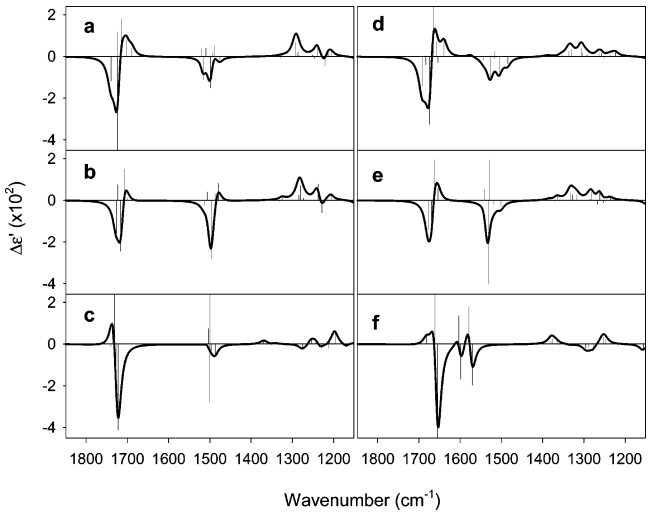

Figure 4. Fully DFT simulated VCD spectra for the model isolated and solvent-perturbed peptides. Isolated peptides (left): (a) α-helical **A7**, (b) 3_{10}-helical **T5**, and (c) 3_1-helical **P5**. Solvated peptides (right): (d) α-helical **A7W**, (e) 3_{10}-helical **T5W**, and (f) 3_1-helical **P5W**. Band intensity is differential molar extinction coefficient per amide group. Vertical lines are proportional to rotational strengths of components

in agreement with observations,[48] there is more variation (components with opposite signs) for the 3_1-helix amide III.

The DFT VCD for the solvated α- and 3_{10}-helices (**A7W** and **T5W**, respectively) are subject to the same frequency shifts as the IR with respect to the corresponding isolated peptides, but since the band shapes and intensities essentially move with the IR transitions, the band shapes are predicted to be roughly constant, particularly for the amide I. For the 3_1-helix, **P5W**, the negatively biased negative couplet amide I VCD is again predicted, but is distorted. The solvated 3_1-amide II becomes more complex, yielding two negative couplets, and more intense than predicted for **P5**. The couplet shape (sign pattern) suggests the experimental result (Figure 1c), if the former were greatly broadened. The C_α-H and amide III modes remain net positive with some band shape fluctuation, especially for **P5W**, and some loss in overall intensity in comparison to the isolated molecule simulations.

Spectra of Large Oligopeptides Simulated by Transfer of Parameters. Simulated gas-phase IR spectra for the 21-amide oligopeptides, α-helical **A21**, 3_{10}-helical **T21**, and 3_1-helical **P21**, are shown in Figure 5. These spectra were calculated using the parameters transferred from the **A7**, **T5**, and **P5** peptides, respectively. Also shown in Figure 5 are the simulated IR spectra for "solvated" large oligopeptides, **A21W** (α-helical) and **T21W** (3_{10}-helical) and **P21W** (3_1-helical). As explained above, these solvated large models do not explicitly contain solvent molecules, but their spectral parameters are transferred from the explicitly solvated smaller peptides **A7W** (α-helix), **T5W** (3_{10}-helix), and **P5W** (3_1-helix). Therefore, as demonstrated in the Discussion section, the transferred vibrational parameters and the resulting simulated spectra contain all the relevant peptide−water interaction terms. Comparison of VCD spectra for these isolated and solvated large peptide models is shown in Figure 6. Overall the computed IR and VCD spectra for these long helices reflect the features seen in the simulated spectra for the corresponding shorter models for which the spectral parameters were computed at full DFT level. The longer oligopeptide spectra generally have narrower, more uniform IR bands dominated by one or a few modes whose composite intensity is due to exciton coupling of amides within these longer, more regular structures, which have a greater repeat length and smaller

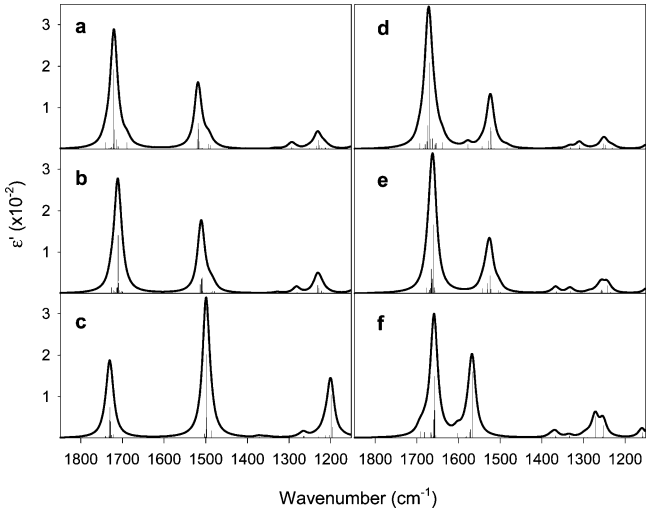

Figure 5. Simulated IR spectra for the longer peptides obtained by transfer of the DFT calculated parameters from shorter fragments. Isolated peptides (left): (a) α-helical **A21**, (b) 3_{10}-helical **T21**, and (c) 3_1-helical **P21**. Corresponding solvent perturbed peptides (right): (d) α-helical **A21W**, (e) 3_{10}-helical **T21W**, and (f) 3_1-helical **P21W**. Intensities plotted as in Figure 3.

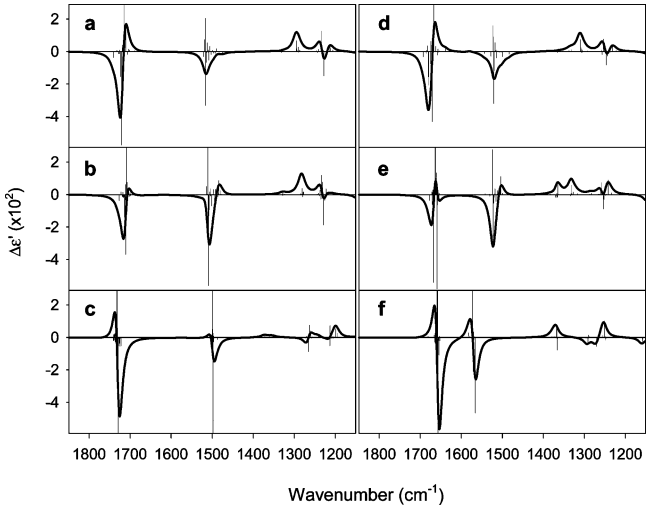

Figure 6. Simulated VCD spectra for the longer peptides obtained by transfer of the DFT calculated parameters from shorter fragments. Isolated peptides (left): (a) α-helical **A21**, (b) 3_{10}-helical **T21**, and (c) 3_1-helical **P21** and corresponding solvent perturbed peptides (right): (d) α-helical **A21W**, (e) 3_{10}-helical **T21W**, and (f) 3_1-helical **P21W**. Intensities plotted as in Figure 4.

contribution from the end residues. Such narrowing is seen experimentally in homopeptides with regular structures and long persistence lengths and is consistent with the helix approaching an infinite periodic (1-D crystal-like) structure.[20,49,50] In the **A21** and **T21** simulated spectra, the amide I maximum shifts slightly (~3−5 cm^{-1}) to lower frequency as compared to the **A7** and **T5** small peptide predictions. This also occurs for the solvated α-helical **A21W** and 3_{10}-helical **T21W**. For the 3_1-helical models there were virtually no frequency shifts of the maxima from the smaller fragment values. The amide II IR is again more intense than the amide I for isolated 3_1-helical **P21**, but this is corrected on solvation for **P21W**. Mode dispersion is again less for the 3_{10}- and 3_1-helices, yielding slightly smaller bandwidths.

The resulting long oligopeptide VCD spectra (Figure 6) are again very similar to those of the corresponding shorter peptides (Figure 4), whose DFT-calculated parameters were used for the spectral simulations. In all cases, intense positive couplet amide

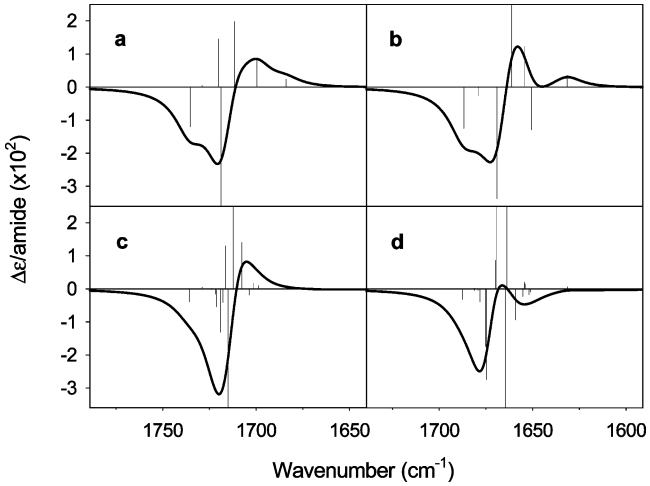

Figure 7. Comparison of simulated amide I′ (N-deuterated) VCD for isolated and solvent perturbed, short (top) and long (bottom) α-helical peptides: (a) **A7**, (b), **A7W**, DFT-level, and (c) **A21**, (d) **A21W,** from transferred DFT parameters. Note shifted frequency scales between the left (vacuum) and right (solvated) panels. Intensities plotted as in Figure 4.

I VCD is predicted for α-helix and even more intense, negative couplet VCD for the 3_1-helix. These amide I VCD bands are also somewhat narrower and sharper than those of the smaller peptides, correlating to the narrower IR absorption bands and resulting in almost doubling the peak VCD intensities on a per residue basis. (In general, the intensities of derivative shaped bands are very sensitive to bandwidth, sharper ones being naturally more intense.) The only qualitative change in the VCD band shape is predicted for the solvated 3_{10}-helical **T21W** oligopeptide, where a negative, low intensity component appears on the amide I, resulting in a distorted "−,+,−" sign pattern. The amide II for 3_1-helical **P21W** is predicted to be a significantly more intense negative couplet than in the other models. The amide III shows the same band shapes as for the shorter models, again weak, distributed over several modes, and predominantly positive.

N-Deuteration. Aqueous solution vibrational spectroscopic experiments are most commonly carried out in D_2O due to the strong absorption of H_2O in the amide I spectral region. In D_2O the peptides become N-deuterated as a consequence of H/D exchange of the amide protons with solvent. The N-deuteration causes small frequency shifts of the amide I′ band (N-deuterated species) with respect to the amide I (N-protonated) and results in some qualitative changes in VCD band shapes. Experimentally, for α-helical structures, the positive couplet amide I VCD changes into a 3 peak (−,+,−) amide I′ pattern (Figure 1a).[51−54]

To study these effects, spectral simulations were performed for the α-helical oligopeptide models with N-deuterated amide groups. In all cases the IR spectra (not shown) exhibit the amide I′ maximum shifted lower in frequency by 4−5 cm^{-1}, directly corresponding to experimental results. More interesting effects can be seen in the simulated amide I′ VCD, shown in Figure 7 for the α-helical oligopeptide models **A7**, **A7W**, **A21**, and **A21W**. Other than the small frequency shift, corresponding to the shift of the absorption maximum, there is virtually no effect of N-deuteration on the amide I′ VCD of the **A7** (Figure 7a). While the **A7W** (Figure 7b) amide I′ retains its basic positive couplet shape, a negative VCD component appears on the low-frequency side of the positive band. Similarly, the isolated **A21** amide I′ (N−D) does not evidence any qualitative change in the VCD band shape (Figure 7c) compared to the amide I (Figure 6a), but is somewhat weaker and more negatively biased.

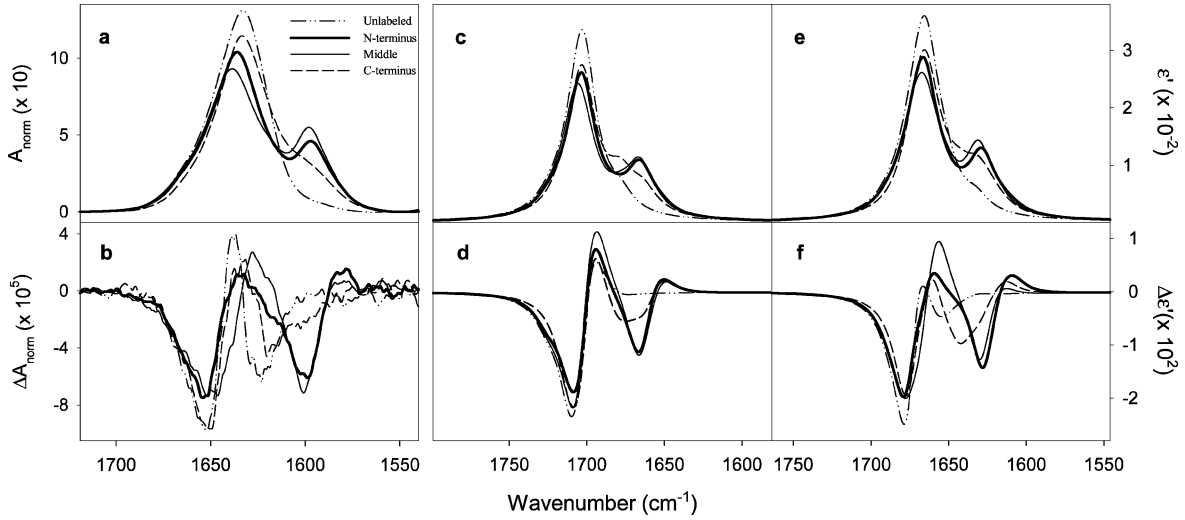

Figure 8. Experimental and simulated amide I′ IR and VCD spectra for ^{13}C isotopically labeled α-helical peptides. All unlabeled (**U**, **U21**, **U21W**) peptides are represented by thin dash−dot-dot line, N-terminally labeled (**N**, **N21**, **N21W**) by thick solid line, middle labeled (**M**, **M21**, **M21W**) by thin solid line, and C-terminally labeled (**C**, **C21**, **C21W**) by a dashed line. (a) experimental IR, (b) experimental VCD, (c) simulated IR, and (d) simulated VCD for isolated models; (e) simulated IR and (f) simulated VCD for solvated models. Note the shift on the frequency axis between panels c and d (vacuum simulations) and panels e and f (solvated peptide simulations).

By contrast, the solvated α-helical oligopeptide **A21W** (Figure 7d) now shows a distinct (−,+,−) amide I′ VCD sign pattern, which provides a much better qualitative agreement with the VCD band shape seen in D_2O-based experiments than does **A21**.[51−54]

^{13}C Substitution. Comparison of the experimental IR and VCD amide I′ spectra for a series of Ala-rich peptides with variably placed sequences of four residues, ^{13}C substituted on the amide C═O, and corresponding simulated spectra for α-helical 20-residue peptides with and without solvent, is presented in Figure 8. Experimental IR and VCD spectra for these ^{13}C labeled α-helical oligopeptides were reported previously and compared with DFT-based spectral simulations for isolated (no solvent) model peptides.[12] However, in the earlier study the peptide models for theoretical simulations of spectra were based on DFT-optimized helical geometries (obtained with decapeptides[17]), while here the DFT optimizations were constrained to idealized regular helical (ϕ,ψ) parameters (Table 1).

The experimental spectra were measured at 5 °C, where the peptides are predominantly α-helical. To emphasize the spectral differences due to different label positions, the amide I′ bands for different isotopomers are overlaid. The unlabeled, **U**, peptide shows the amide I′ absorption maximum at ∼1633 cm^{-1}, which is typical for short isolated α-helical peptides in aqueous solutions.[55−57] Experimentally, the **N** and **M** peptides give relatively similar amide I′ IR spectra with the main ^{12}C peak, ∼1636−1639 cm^{-1}, and a weaker, resolved ^{13}C peak at ∼1597−1600 cm^{-1}. A qualitatively different amide I′ is observed for the **C** peptide, where the main ^{12}C band is the most intense of the labeled peptides and occurs at the same frequency as that for **U**, while the ^{13}C band is just a broadened shoulder. Small differences, however, are seen between the **N** and **M** experimental IR spectra. The **N** amide I′ has the most intense ^{12}C band and weakest ^{13}C band, which appears at the lowest frequency among all the labeled peptides (1597 cm^{-1}). The ^{12}C amide I′ of **M** has the highest frequency (1639 cm^{-1}), while the ^{13}C band is only slightly higher than that for the **N** peptide, resulting in the largest separation between the ^{12}C and ^{13}C peaks (∼41 cm^{-1}) for **M**. **M** has also the most intense ^{13}C band.

The VCD spectra for all these peptides show characteristic α-helix features (Figure 1a) that result in an intense, (−,+,−) 3-peak spectral band over the ^{12}C amide I′ region.[51−54] Just as for the high-frequency negative VCD lobe with respect to the main ^{12}C IR band, the lower negative lobe for **N** and **M** is to the high-frequency side of the ^{13}C induced IR band and is accompanied by a weak positive band at ∼1580 cm^{-1}. The **C** VCD is again most similar to that of **U**, yielding a less dispersed pattern, with the ^{13}C negative band appearing as a shoulder on the ^{12}C component. The differences between **N** and **M** in the VCD are much less obvious than in the IR, with the central positive VCD band being shifted down for **M**. The **N** has the most intense low-frequency positive ^{13}C component.

A subtle but important feature of these experimental spectra is the different relative intensities of the ^{12}C and ^{13}C bands depending on the label position and, especially, an apparent enhancement of the ^{13}C band intensities in the labeled peptide VCD. The integral IR intensity of the ^{13}C band, estimated by band-fitting, approximately corresponds to the fraction of the labeled amide groups, about 19%, except for **M** where it is slightly higher (∼24%). However, in all cases except **C**, the relative (integral) VCD intensity of the ^{13}C signal is much larger than expected according to the proportion of the labeled groups, nearly 35% for **M** (more than 50% of the ^{12}C intensity) and about 30% for **N**.

In agreement with our earlier results,[12] most of the relative variations in IR and VCD spectra between different ^{13}C isotopomers are reproduced in the simulated spectra for the isolated α-helical peptide models (Figure 8c, d). Overall, however, the predicted differences between peptides with different labeling patterns are smaller than seen experimentally. In the IR the C-terminally labeled **C21** spectrum is different from the others, although the simulated ^{13}C shoulder appears more resolved and intense than in the experiment. This is expected due to the fraying of the C-terminal segment in aqueous solution, which is not encompassed in the model.[12] The ^{13}C band in **N21** is predicted at the lowest frequency and to be less intense than for **M21**, while for the ^{12}C band, **N21** has more intensity and **M21** is higher in frequency, both qualitatively matching the experimental results. Using the vacuum parameters,

TABLE 3: Comparison of $^{13}C{=}O$ Mode Frequency, Symmetry, and Coupling for Variable Separations Computed with the A21W α-Helical Peptide[a]

peptide notation	isolated (vacuum)			solvated N−H				solvated N−D		
	ip	oop	split, 2V	notation	ip	oop	split, 2V	ip	oop	split, 2V
2LT	1679.9	1666.0	13.9	2LTW	1634.8	1621.2	13.6	1629.3	1618.1	11.2
2L1S	1669.9	1674.1	−4.2	2L1SW	1624.8	1629.5	−4.7	1620.3	1626.0	−5.7
2L2S	1670.3	1673.6	−3.3	2L2SW	1624.5	1629.6	−5.1	1620.5	1625.7	−5.2
2L3S	1672.4	1671.5	0.9	2L3SW	1627.7	1626.2	1.5	1623.7	1622.2	1.5
2L4S	1656.4	1657.6	−1.2	2L4SW	1626.3	1627.6	−1.3	1622.1	1623.8	−1.7

[a] Notation (oop) out of phase, (ip) in phase, coupling: $V = \Delta\omega/2$; all values in cm^{-1}.

the calculated amide I′ VCD for the unlabeled **U21** is a positive couplet, compared to a three peak (−,+,−) experimental amide I′ VCD. The **C21** amide I′ is again closest in shape to the **U21**, however, as in the IR, the ^{13}C VCD amide I′ band of **C21** is more resolved and intense than in the experiment since it, like all the segments, is helical, not frayed, in the simulation. Compared to the experiment, the negative ^{13}C VCD intensities of **N21** and **M21** are computed to be a bit weaker with respect to the ^{12}C negative VCD, but the ^{12}C positive band is correctly predicted to be more intense for the **M21** than for **N21**. The low-frequency ^{13}C positive VCD, characteristic of an α-helix, is predicted for all labeled species.

Although the relative ^{13}C VCD intensity is larger than would be expected for the fraction of labeled residues, the vacuum simulation underestimates the enhancement of the ^{13}C signal seen experimentally. The intensities of the ^{12}C and ^{13}C band components were estimated by band fitting and integration of the components. The largest relative ^{13}C VCD intensity is predicted for the N-terminally labeled **N21** (∼35% of the total intensity of the amide I′ band) while experimentally the strongest ^{13}C VCD was observed for middle labeled **M** peptide. By contrast, stronger ^{13}C absorption than observed is predicted in the IR for **N21** (∼ 29%), while that for the **M** corresponds to the experimental value of ∼24%.

By contrast, calculated amide I′ vibrational frequencies for the solvated isotopically labeled peptides (Figure 8e) are much closer to experimental values than their isolated counterparts, although they are still about 30 cm^{-1} higher than the experiment. However, the IR amide I′ band shapes for the solvated isotopically substituted model peptides (except for **U**) are qualitatively the same as for the isolated models, just shifted down by ∼40 cm^{-1}. The differences in ^{13}C IR and ^{12}C VCD band intensity between the **N21W** and **M21W** have a better match to the experimental results than do the vacuum simulations. Better agreement with experiment can also be observed in the simulated peptide plus solvent VCD band shapes (Figure 8f). The **U21W** shows a clear three-component (−,+,−) amide I′ VCD band shape and the labeled peptides show a somewhat more intense ^{13}C negative band compared to the ^{12}C one than do the vacuum simulations. **N21W** is predicted to have a significantly more intense positive ^{13}C band than **M21W**. The shapes of the ^{12}C central positive bands, which are less intense and broader for **N21W** and more symmetric and intense for **M21W**, also correspond well to the experiment. The level of detail discussed above approaches the limits of our experimental reliability, leading to the conclusion that the quality of detailed agreement with theoretical prediction is quite remarkable. Quantitatively, the **N21W** negative ^{13}C VCD intensity is estimated by band fitting to be ∼45% of the total band area, which is actually greater than seen experimentally (∼30%). On the other hand, the 33% relative ^{13}C band intensity in **M21W** is essentially the same as seen experimentally (35%).

Prediction of polymer band shapes, both IR and VCD, depends on the relative intensity distribution of the components of a band and their splitting, which is due to interresidue coupling. While for a uniform polymer of infinite length, the lines can be narrow with only a few exciton components having intensity, for oligomers many components will retain intensity and the dispersion of modes will contribute to the experimentally observed band profile. (For nonuniform oligomers, band shape is an even more complex issue, but one we have not addressed in this work.) For VCD, the relative angles of the coupled modes, basically fixed by the conformation, are also important. To explore specifically the effect of coupling, we previously studied the IR and VCD of 25-residue peptides with two ^{13}C-labeled amides progressively more separated along the helix, the **2LT** and **2LnS** models.[20] As a test of the effect of solvation on this coupling, we simulated the spectra for a correspondingly labeled set of 20 residue α-helical peptides. Simulated coupling constants for the ^{13}C amide I (amide I′ for N−D) modes are shown in Table 3. From these values it is clear that, although the solvated amide I modes shift down in frequency as expected, the general magnitude of the splitting (and sign of the coupling) between the two $^{13}C{=}O$ modes is virtually independent of perturbation by explicitly included water. In other words, the resultant ^{13}C IR band shapes are nearly identical to those obtained previously, with the exception of slightly increased intensity and width.[20] It is this amide-centered, peptide-dependent coupling that leads to the consistent conformational dependence of amide IR and VCD that has been seen experimentally in various solvation environments which result in various amide I frequencies yet lets the band shape shift with the frequency.

In Figure 9 simulated amide I (N−H) and amide I′ (N−D) IR and VCD spectra for the **2LTW**, **2L1SW**, and **2L2SW** peptides are compared to experimental amide I′ (in D_2O) IR and VCD spectra for the analogous 25-mer alanine peptides at 5 °C.[20] The VCD shapes predicted here for these ^{13}C isotope substituted peptides solvated with water are nearly identical to the same peptides in vacuum (previously reported,[20] not shown), aside from a slight increase in intensity for the $^{13}C{=}O$ bands. The $^{13}C{=}O$ VCD yields a distinct couplet that remains opposite in sign for the solvated **2LTW** and **2L1SW**, as seen experimentally, that reflects the sign of the coupling, V. The ^{13}C contribution to the VCD is too small to be measured for the **2L2SW** and **2L3SW** variants (some baseline drift below 1600 cm^{-1} is evident in the experimental **2L1S** and **2L2S** VCD in Figure 9). Deuteration is predicted to have a surprising impact on the ^{12}C VCD, which is partly a function of the line width used for simulation.

Other than an approximately 5 cm^{-1} shift down in frequency, N-deuteration has little effect on the amide I IR of these labeled species, but of course shifts the amide II from ∼1530 cm^{-1} to roughly 1430 cm^{-1}. For VCD the effect is more complex. Adding a negative going feature between variably signed but weak ^{13}C VCD components makes the result highly dependent on overlap of band features. For **2LT** and **2L1S** the ^{13}C VCD components are still predicted, but the lower frequency negative

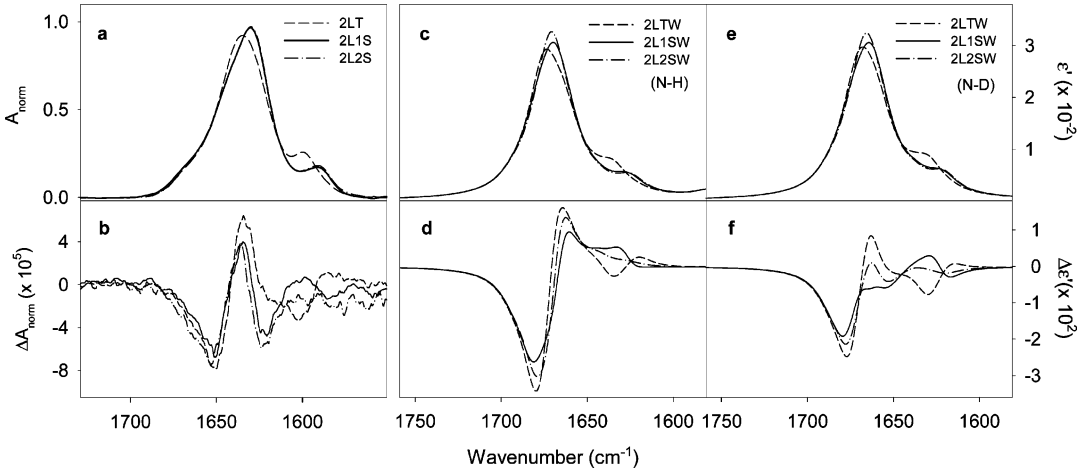

Figure 9. Comparison of experimental amide I′ (in D_2O) for doubly ^{13}C isotopically labeled alanine 25-mer peptides with variable label separations, and simulated amide I (N−H) and amide I′ (N−D) spectra for solvated 21-amide α-helical models. Peptides with adjacent ^{13}C labels (**2LT**, **2LTW**) are represented by a dashed line, ^{13}C labels separated by one unlabeled residue (**2L1S, 2L1SW**) by a solid line, and ^{13}C labels separated by two unlabeled residues (**2L2S, 2L2SW**) by a dashed−dot line. (a) experimental IR, (b) experimental VCD, (c) simulated amide I (N−H) IR and (d) simulated amide I (N−H) VCD, (e) simulated amide I′ (N−D) IR, and (f) simulated amide I′ (N−D) VCD.

TABLE 4: Comparison of ^{13}C═O Mode Frequency, Symmetry, and Coupling for Variable Separations in Solvated 3_1-Helical Peptide (P21W)

peptide notation	N−H			N−D		
	ip	oop	splitting 2V	ip	oop	splitting 2V
2LTW	1621.5	1613.9	7.6	1613.1	1610.0	3.1
2L1SW	1616.9	1618.3	−1.4	1610.6	1612.5	−1.9
2L2SW	1618.1	1617.0	1.1	1611.9	1611.0	0.9
2L3SW	1617.4	1617.8	−0.4	1611.3	1611.6	−0.3
2L4SW	1617.6	1617.6	0.05[b]	1611.5	1611.4	0.1

[a] Notation (oop) out of phase, (ip) in phase, coupling: $V = \Delta\omega/2$; all values in cm^{-1}. [b] Difference determined in higher precision.

is emphasized and the positive weakened by the overlap with the new (N−D originating, as shown for no labels in Figure 7) ^{12}C lower frequency negative branch. The **2LT** is predicted to have two negative components between the positive lobes, with the lower one more intense, just as seen experimentally. The **2L2S** prediction however, suggests a stark reduction in intensity for the central positive lobe, in only qualitative agreement with the reduction seen.

Finally, when these helical peptides are heated, the IR of the ^{13}C amide I band seem to virtually disappear into the shoulder of the broadened ^{12}C band corresponding to the disordered species (generally assigned to be 3_1 helical or polyProII-like). In VCD it corresponds to a weak broad negative shoulder, as seen earlier in the tetra-labeled cases.[12] Our simulation of the spectra for these labeling patterns in 3_1 helices show all to be the same; little variance is found in terms of frequency or intensity. All have a negative VCD corresponding to the low-frequency side of the ^{13}C absorbance maximum, which is shifted about 40 cm^{-1} down from the ^{12}C maximum. Deuteration seems to have little effect on the predicted band shape, other than the ∼5 cm^{-1} frequency shift. Surprisingly the ^{13}C═O splitting in **2LT** reduces to about half its value for the protonated peptide, possibly due to some near resonant mixing with ^{12}C═O modes. The effects of coupling are much smaller for the 3_1-helix but show sign changes for the **2L1S** and **2L3S**, whose patterns and differences from the α-helix may reflect the periodicity change (3_1 as opposed to 3.6_1 for the α-helix). These are summarized in Table 4. This weaker coupling in **2LT** is the nearest neighbor effect and is partly responsible for the narrower line widths predicted for 3_1-helices. These are only seen experimentally in polyPro systems where a uniform structure develops. The same phenomenon underlies the lower intensity VCD characteristic of the 3_{10}-helix, where the ^{13}C═O splitting in **2LT** (∼4 cm^{-1}) is predicted to be about 1/3 that for the corresponding α-helix.

Discussion

The above results demonstrate the most significant effects on the vibrational spectra of helical oligopeptides that can be expected due to interaction with water. The initial layer of hydrogen bonded water poses the most significant perturbations on the amides and their vibrational spectra. The frequency shifts determined by including the water perturbations in the DFT-based spectral simulations reflect most of the common solvent effect, and bring the amide I and II modes into significantly improved agreement with experiment. However, a more important result is that the band shapes of the VCD and the splittings of the IR bands are not seriously affected by these strong solvent perturbations. The level of agreement obtained here between experiment and simulation is very high, particularly for mode-sensitive experiments such as isotopic labeling. The level of spectral detail being reflected by these simulations is at the limit of our ability to measure VCD band shapes for aqueous phase peptides.

As described in the Methods section, the spectra for these solvated oligopeptides were actually simulated for the peptide alone, without including the coordinates and parameters for the water molecule atoms, but by using the solvent-perturbed spectral parameters obtained from DFT calculations for the complete peptide−water complex. This approach was chosen to avoid interference of the HOH bending vibrations in the amide I region, which obscures the resulting simulated spectra and thus complicates the comparison to the isolated peptide simulations and to experiment, even if the intensity parameters (APT and AAT) for the water atoms are set to zero.[13]

While vibrational coupling between the amide and water vibrational modes has been observed experimentally,[58,59] we have chosen not to address that problem since the model peptide−water complexes used here are unlikely to provide good representation for such effects. First, the computed spectra are for one particular configuration of hydrogen-bonded waters, while experimentally their contribution is averaged over an ensemble of local structures, which is a consequence of the weak hydrogen bonding potential with relatively shallow minima.

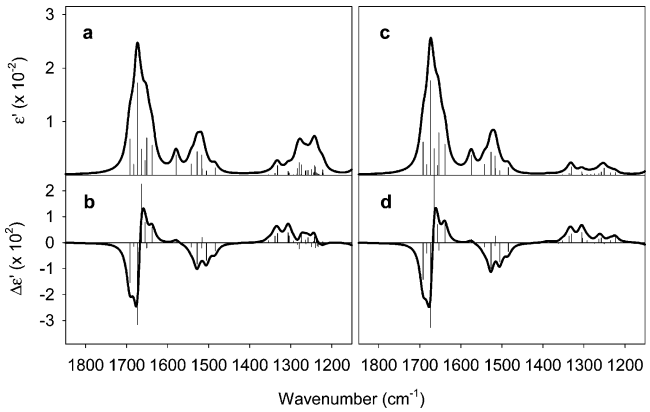

Figure 10. Test of the parameter transfer method for simulation of solvated peptide spectra. Comparison of the full DFT-level simulation of IR (a) and VCD (b) spectra for α-helical heptaamide-D_2O complex with corresponding IR (c) and VCD (d) spectra simulated by transfer of vibrational parameters from fully solvated DFT calculation onto the α-helical heptaamide without explicit solvent molecules (**A7W**).

Second, only the minimal number of H_2O molecules, corresponding to the first hydration sphere, have been used here to make the computational requirements reasonable. Due to the interactions with additional surrounding solvent molecules, the solvent structure around the peptide molecule will vary[23,24] as evidenced experimentally for peptides and proteins in H_2O, after subtraction of the solvent spectrum, by their overall broader amide I, even though no vibrational structure originating from water remains evident.[9,23] The resulting complex, multicomponent amide I bands that arise in peptide-discrete H_2O simulations are effectively computational artifacts due to consideration of just a single water configuration. (This could be addressed by calculating spectra for the peptide in a bath of water molecules, using molecular dynamics, but DFT determination of the FF would not be possible, and some parametrized model would be needed.[23,60−62])

The most common alternative way of removing the interference of water modes is by deuteration or use of a different solvent, as is often done experimentally. We could have computed the spectra for explicit peptide−water complexes and subsequently removed the undesired solvent interference by deuteration (converting H_2O to D_2O). However, as demonstrated in Figure 10, the fully DFT simulated spectra for the optimized solvated α-helical heptaamide−D_2O complex have virtually identical band shapes, mode distributions, and component intensities (for the amide I and II bands) as do those simulated for the peptide alone (no water) but with the peptide-only FF, APT, and AAT parameters transferred from the solvated DFT calculation. The amide III region does differ due to the DOD bending motion interference there. While simulation with D_2O leads to the same amide I−II spectra as transfer of parameters from the solvated peptide to only the peptide molecule, for the large oligopeptides the computation is simplified, and efficiency enhanced, by not including explicit water molecules. This provides the rationale for our method of transfer of solvated peptide parameters only, which is done in both the long and short model peptide simulations, for consistency.

While the amide vibrational frequencies shift significantly as a result of interaction with solvent, the computed VCD band shapes are relatively stable. This is a direct consequence of VCD originating from chiral coupling between the amide groups, which depends only on the relative orientation of those groups, a natural consequence of the conformation of the peptide chain. More specifically, those normal modes that make the biggest VCD contributions have the same relative frequency ordering, which occurs because the coupling constants are only weakly perturbed by the solvation, as demonstrated in our isotopic labeling experiments and computations and discussed below.

The predicted amide I and II frequencies correlate strongly with the hydrogen bond formation by the amide groups, both intramolecular in α- and 3_{10}-helices, and with solvent, as we show here. In all cases the amide I frequencies are systematically predicted too high compared to the experimental values, while the amide II frequencies are too low. These discrepancies come predominantly from neglect of the solvent interactions in the calculations, as best seen from the solvated oligopeptide spectral simulations above. Although our calculated frequencies with solvent are still off from those observed in aqueous solutions, this is an obvious consequence of using just a minimal solvent model, containing only a few hydrogen-bonded water molecules. Additional solvent molecules, interacting with the first hydration sphere would cause further low-frequency shifts as has been observed, for example, with single amide model calculations, such as for NMA.[9,23,24,60,63] Similarly, larger basis sets, particularly including diffuse orbitals, would lead to better representations of hydrogen bonds and of the amide I frequencies.[9,44] Including additional layers of explicit waters would become prohibitively expensive for DFT calculations on peptides of the size considered here, but empirical correlations suggest that the solvent electric field of the peptide can provide a useful parameter for taking solvation effects into account.[60,63]

It has been shown that the electrostatic field of the bulk solvent has a significant impact on computed amide vibrational frequencies[9,23−25,33] and can also induce amide vibrational frequency shifts in non-hydrogen bonding solvents, even low polarity ones, compared to the gas phase. This has been observed for model amides both experimentally[9] and computationally.[23] The strong dependence on polarity of the environment moreover suggests that the frequencies are likely to be affected not only by solvent but also by the local environment resulting from polar and/or nonpolar sidechains. In addition, the residue sidechains can mediate the solvent accessibility of the amide groups. These nonconformational effects are not taken into account in the model used here, but have been seen in model hairpin calculations which include empirical corrections for side chains (Bour and Keiderling, unpublished results). Naturally, sidechain effects combined with solvation represent much more computationally demanding problems, particularly at the DFT level. However, quantitative understanding of such effects may be important for accurate interpretations of vibrational spectra of peptides and proteins and is the objective for the future stages of our continuing combined computational and experimental investigations of peptide and protein structure−spectra correlations.

The VCD band shapes, on the other hand, are little affected by these factors, and even vacuum, isolated molecule calculations give qualitatively correct results. The only simulated change of VCD band shape upon solvation was for the amide I of the 3_{10}-helix (Figure 6f). While such a band shape has not been experimentally observed, comparison with experiment is particularly problematic for the 3_{10}-helix. Most 3_{10}-helical oligopeptide models are relatively short peptides that contain α-methylated residues and are not soluble in water. The α-methylation causes some qualitative changes in the VCD band shapes, especially in the amide I.[16] Moreover, even with α-methylated amino acids, the longer peptides, approximately above 10 residues, show a preference for the α-helix formation.[64−68] Thus, experimental VCD spectra do not exist for either long 3_{10}-helical oligopeptides or 3_{10}-helices without α-meth-

ylated residues, or for 3_{10}-helices in aqueous solution (IR of these have been measured in various approximations but offer little in the present comparison). Thus the band narrowing effects of the reduced near-neighbor coupling in 3_{10}-helices cannot be easily tested except through the lower intensity amide I and higher amide II VCD that is characteristic of this structure. The sign variation of VCD, much as seen in the α-helix models,[20] is an important source of experimental determination of these coupling parameters.

The stability of the computed VCD band shapes is due to the fact that the ordering of the normal modes of vibrations is not significantly affected by the solvent. In general the most intense amide I modes for both IR and VCD arise from delocalized vibrations involving most of the amide groups in the helix, except the terminal groups. The vibrational frequencies of these major components of the exciton band tend to be in approximately the same relative order, even when solvated, because they reflect the basic coupling of the amides in the polymer chain, which is little changed by solvation, as seen in our selectively isotopically labeled peptide tests. In the α- and 3_{10}-helical models, the N-terminal amide groups consistently have lower frequencies than the ^{12}C amide I, and C-terminal amide groups appear on the high-frequency side. For the amide II the situation is approximately opposite, the N−H hydrogen bonded C-terminal groups contributing to a high-frequency component of the band. By contrast for the 3_1-helix there seems to be no preference, both ends contribute to high and low-frequency amide I modes. The smaller coupling between the 3_1-helical vibrations (Table 4, also for 3_{10}-helices, not shown) is evidenced by generally smaller normal mode dispersion within the band.

Several recent reports have emphasized a perceived need to determine better diagonal force constants in order to interpret the weaker couplings that lead to 2-D IR and VCD.[62,69] While absolute accuracy is a worthwhile goal, especially determining the origins of how the observed frequencies depend on conformation, our results show that it is not a necessary condition for interpretation of relative band shapes which are primarily dependent on couplings. Thus certainty regarding diagonal force constants is not required to interpret VCD or probably other coupling-related experimental data, such as 2-D IR and splittings of Raman polarization components.[70−72] However, one must be careful to avoid misinterpretations of end effects and the like where the impact of solvent might be unique.

One of the challenges for peptide VCD spectra simulations has been to reproduce the three-peak, (−,+,−)-shaped amide I′ for N-deuterated α-helical peptides.[51−54] Such a pattern was computed once before, for an Ala triamide model with five explicit hydrogen bonded molecules.[13] However, this band shape was predicted for both N-protonated amide I as well as N-deuterated amide I′ VCD. The present study is thus the first time a couplet amide I band shape and, after deuteration, a (−,+,−) amide I′ were consistently obtained from the same DFT level FF, APT, and AAT simulations using our methods. Using an empirically corrected scheme, Choi and Cho have also modeled this band shape (Choi J.-H., Cho, M. H., personal communication).

It is interesting to note that the (−,+,−) amide I′ band shape is not very clear for the solvated shorter fragment **A7W** (Figure 7b), but is developed to an experimentally realistic form after transfer of those parameters onto the long **A21W** oligopeptide. Thus, although based on the above results this (−,+,−) band shape would appear to be due to interactions with solvent, the higher order intrahelical interactions between the amide groups in the longer α-helical segment must also contribute. This subtle spectral signature may thus contain information about the length of the helical segment. Studies of α-helical polypeptides, with longer helical segments, give added weight to this suggestion.[10,53,73,74,49,75]

The experimental and computational results for ^{13}C isotopically substituted helical peptides show distinct spectral patterns, dependent on the positions of the ^{13}C labeled residues within the helix. As noted above, in general, the normal modes from different portions (termini) of the α-helix tend to contribute to different components of the amide band. The modes localized at the N-terminus of the peptide tend to be computed with lower frequency. This can be understood from the fact that C═O groups point toward the C-terminus, therefore the N-terminal C═O points toward the rest of the helix and is subject to the strongest H-bonded interaction with other amides. The N−H groups on the C-terminus are not H-bonded to other amides and no electrostatic interactions can balance that deficiency. The major electrostatic factor relates to the helical macrodipole, which for an α-helix has a positive pole on the N-terminus[76,77] and would strengthen the C═O bond, which has a partial negative charge on the O and is oriented in the opposite direction. The intense modes near the band center, on the other hand, are delocalized modes involving amide groups from the central portion of the helix. The C-terminal groups contribute on the high-frequency side. The solvent interactions change the mode ordering somewhat, particularly for the fully exposed end groups, but the basic patterns stay the same. This is perhaps best reflected by the relative stability, aside from the frequency shift, of both the IR and, especially, the VCD band shapes between the solvated and isolated peptide simulations.

These patterns are also consistent for ^{13}C labeling of particular segments of the polypeptide. For example, the ^{13}C band is lowest in frequency for N-terminally labeled peptides, most intense for middle labeled ones, and only partially resolved for the C-terminally labeled peptides. The critical aspect for maintaining these band shapes is that the coupling between specific sites is not significantly modified by solvation. Thus the diagonal FF components are changed, the spectra shift, but the off-diagonal, at least on a local scale of a few residues, is relatively constant so the splittings between coupled modes (in our case the two labeled ^{13}C═O groups) are maintained and the VCD signs preserved.

An important characteristic of these isotopically labeled spectra is the nonadditivity of the intensities for the ^{12}C and ^{13}C labeled parts in both IR and, more significantly, in the VCD. The intensity of the ^{13}C originating VCD bands is much higher (nearly double) than suggested by 19% labeling of the amide chromophores. This enhancement, since it is much smaller in the experimental high temperature and the computed 3_1-helical spectra,[12] is also conformationally sensitive. Such amplification implies that site-specific labeling has broader potential since a relatively small amount of label may be detected experimentally if it is in a helix, leading to more sensitivity to stereochemistry. The ^{13}C band intensities are underestimated in most of the simulations, particularly for the isolated molecules, although an enhancement over the statistical weight of the labeled residues is predicted in all cases. Larger enhancements are calculated in the solvated models, where also the qualitatively correct "−,+,−" amide I′ band shape provides a better agreement between the theoretical and experimental VCD.

The fundamental characteristic that leads to the ability to use vacuum calculations to simulate solution phase spectra, IR band

profiles (splitting), and VCD band shapes (sign patterns) is the consistency of interresidue coupling independent of environment and of diagonal force constant. The isotope experiments, where two labeled residues are in various relative positions in the sequence, are the critical demonstration of this property showing this to be true. The corresponding calculations demonstrate that consistency to be an underlying property of the simulations. Until such solvated models could be calculated, it was not possible to clearly assign the root cause for the experimentally observed spectral stability. Now that we have it, the vacuum calculations can be seen to have definite value in prediction of spectral patterns.

Conclusion

DFT-based simulations of IR and VCD for oligopeptides up to 21 amide groups in α-, 3_{10} and 3_1-helical conformations and including explicit solvent demonstrate the potential effects of aqueous solvent on oligopeptide vibrational spectra. The solvent substantially influences the amide band vibrational frequencies, shifting them closer to the experimental values, but the characteristic VCD band shapes stay relatively constant. As a consequence, while conformational analysis based on IR amide absorption frequencies alone has been known to be complicated and often misleading, VCD is largely unaffected by nonstereochemical frequency shifts and thus provides more reliable conformational probe. These theoretical results are in full agreement with experimental results from different solvent environments. Furthermore, theoretical simulations of VCD spectra are valid and useful for analysis of the experimental results, even when carried out for isolated molecules without regard to the solvent. However, some more subtle features of the VCD band shapes are successfully reproduced only by using the solvated models. This includes the (−,+,−) amide I′ (N-deuterated) VCD pattern for the α-helix, as well as some qualitative intensity patterns for the ^{13}C isotopically labeled α-helical peptides. In addition, quantitative comparison between ^{12}C and ^{13}C intensities in the ^{13}C isotopically labeled α-helical models seems to agree more closely with the apparent experimental ^{13}C intensity enhancements.

Acknowledgment. We gratefully acknowledge Prof. Cynthia J. Jameson for providing the computational time on the PC cluster and Dr. Devin Sears for additional help with using this system. This work was supported in part by grants from the Donors to the Petroleum Research Fund administered by the American Chemical Society and by a grant from the National Science Foundation (CHE03-16014). J.K. was supported as a Dean's Scholar funded by the UIC Graduate College.

References and Notes

(1) Barth, A.; Zscherp, C. *Q. Rev. Biophys.* **2002**, *35*, 369.
(2) Keiderling, T. A. *Curr. Opin. Chem. Biol.* **2002**, *6*, 682.
(3) Goormaghtigh, E.; Cabiaux, V.; Ruysschaert, J. M. Determination of soluble and membrane protein structure by Fourier transform infrared spectroscopy. I. Assignments and model compounds. In *Subcellular Biochemistry*; Hilderson, H. J., Ralston, G. B., Eds.; Plenum: New York, 1994; Vol. 23, p 329.
(4) Jackson, M.; Mantsch, H. H. *Crit. Rev. Biochem. Mol. Biol.* **1995**, *30*, 95.
(5) Haris, P. I. Fourier Transform Infrared Spectroscopic Studies of Peptides: Potentials and Pitfalls. In *Infrared Analysis of Peptides and Proteins: Principles and Applications. ACS Symposium Series.*; Ram Singh, B., Ed.; American Chemical Society: Washington, DC, 2000; p 54.
(6) Eaton, G.; Symons, M. R. C.; Rastogi, P. P. *J. Chem. Soc., Faraday Trans. 1* **1989**, *85*, 3257.
(7) Mayne, L. C.; Hudson, B. *J. Phys. Chem.* **1991**, *95*, 2962.
(8) Torii, H.; Tatsumi, T.; Kanazawa, T.; Tasumi, M. *J. Phys. Chem. B* **1998**, *102*, 309.
(9) Kubelka, J.; Keiderling, T. A. *J. Phys. Chem. A* **2001**, *105*, 10922.
(10) Keiderling, T. A. Peptide and protein conformational studies with vibrational circular dichroism and related spectroscopies. In *Circular dichroism: principles and applications*, 2nd ed.; Nakanishi, K., Berova, N., Woody, R. A., Eds.; Wiley: New York, 2000; p 621.
(11) Bour, P.; Kubelka, J.; Keiderling, T. A. *Biopolymers* **2000**, *53*, 380.
(12) Silva, R. A. G. D.; Kubelka, J.; Decatur, S. M.; Bour, P.; Keiderling, T. A. *Proc. Natl. Acad. Sci. U.S.A.* **2000**, *97*, 8318.
(13) Kubelka, J.; Silva, R. A. G. D.; Bour, P.; Decatur, S. M.; Keiderling, T. A. Chirality in peptide vibrations. Ab Initio computational studies of length, solvation, hydrogen bond, dipole coupling and isotope effects on vibrational CD. In *Chirality: Physical Chemistry. ACS Symposium Series*; Hicks, J. M., Ed.; Oxford University Press: New York, 2002; p 50.
(14) Kubelka, J.; Keiderling, T. A. *J. Am. Chem. Soc.* **2001**, *123*, 6142.
(15) Kubelka, J.; Keiderling, T. A. *J. Am. Chem. Soc.* **2001**, *123*, 12048.
(16) Kubelka, J.; Silva, R. A. G. D.; Keiderling, T. A. *J. Am. Chem. Soc.* **2002**, *124*, 5325.
(17) Bour, P.; Kubelka, J.; Keiderling, T. A. *Biopolymers* **2002**, *65*, 45.
(18) Hilario, J.; Kubelka, J.; Syud, F. A.; Gellman, S. H.; Keiderling, T. A. *Biopolymers* **2002**, *67*, 233.
(19) Hilario, J.; Kubelka, J.; Keiderling, T. A. *J. Am. Chem. Soc.* **2003**, *125*, 7562.
(20) Huang, R.; Kubelka, J.; Barber-Armstrong, W.; Silva, R. A. G. D.; Decatur, S. M.; Keiderling, T. A. *J. Am. Chem. Soc.* **2004**, *126*, 2346.
(21) Bour, P.; Sopkova, J.; Bednarova, L.; Malon, P.; Keiderling, T. A. *J. Comput. Chem.* **1997**, *18*, 646.
(22) Silva, R. A. G. D.; Yasui, S. C.; Kubelka, J.; Formaggio, F.; Crisma, M.; Toniolo, C.; Keiderling, T. A. *Biopolymers* **2002**, *65*, 229.
(23) Besley, N. A. *J. Phys. Chem. A* **2004**, *108*, 10794.
(24) Frimand, K.; Bohr, H.; Jalkanen, K. J.; Suhai, S. *Chem. Phys.* **2000**, *255*, 165.
(25) Knapp-Mohammady, M.; Jalkanen, K. J.; Nardi, F.; Wade, R. C.; Suhai, S. *Chem. Phys.* **1999**, *240*, 63.
(26) Tajkhorshid, E.; Jalkanen, K. J.; Suhai, S. *J. Phys. Chem. B* **1998**, *102*, 5899.
(27) Han, W.-G.; Jalkanen, K. J.; Elstner, M.; Suhai, S. *J. Phys. Chem. B* **1998**, *102*, 2587.
(28) Creighton, T. E. *Proteins: Structures and Molecular Properties*, 2nd ed.; W. H. Freeman and Co.: New York, 1993.
(29) Guo, H.; Karplus, M. *J. Phys. Chem.* **1994**, *98*, 7104.
(30) Han, W.-G.; Suhai, S. *J. Phys. Chem.* **1996**, *100*, 3942.
(31) Markham, L. M.; Hudson, B. S. *J. Phys. Chem.* **1996**, *100*, 2731.
(32) Kallies, B.; Mitzner, R. *J. Chem. Soc., Perkin Trans.* **1996**, *2*, 1403.
(33) Torii, H.; Tatsumi, T.; Tasumi, M. *J. Raman Spectrosc.* **1998**, *29*, 537.
(34) Sundaralingam, M.; Sekharudu, Y. C. *Science* **1989**, *244*, 1333.
(35) Weiner, S. J.; Kollman, P. A.; Nguyen, D. T.; Case, D. A. *J. Comput. Chem.* **1986**, *7*, 230.
(36) Insight II.; 94.0 ed.; Molecular Simulations Inc.: San Diego, 1997.
(37) Frisch, M. J.; Trucks, G. W.; Schlegel, H. B.; Scuseria, G. E.; Robb, M. A.; Cheeseman, J. R.; Zakrzewski, V. G.; Montgomery, J., J. A.; Stratmann, R. E.; Burant, J. C.; Dapprich, S.; Millam, J. M.; Daniels, A. D.; Kudin, K. N.; Strain, M. C.; Farkas, O.; Tomasi, J.; Barone, V.; Cossi, M.; Cammi, R.; Mennucci, B.; Pomelli, C.; Adamo, C.; Clifford, S.; Ochterski, J.; Petersson, G. A.; Ayala, P. Y.; Cui, Q.; Morokuma, K.; Malick, D. K.; Rabuck, A. D.; Raghavachari, K.; Foresman, J. B.; Cioslowski, J.; Ortiz, J. V.; Stefanov, B. B.; Liu, G.; Liashenko, A.; Piskorz, P.; Komaromi, I.; Gomperts, R.; Martin, R. L.; Fox, D. J.; Keith, T.; Al-Laham, M. A.; Peng, C. Y.; Nanayakkara, A.; Gonzalez, C.; Challacombe, M.; Gill, P. M. W.; Johnson, B.; Chen, W.; Wong, M. W.; Andres, J. L.; Gonzalez, C.; Head-Gordon, M.; Replogle, E. S.; Pople, J. A. Gaussian 98, revision A.6, Gaussian, Inc.: Pittsburgh, PA, 1998.
(38) Perdew, J. P.; Wang, Y. *Phys. Rev. B* **1988**, *33*, 8800.
(39) Perdew, J. P.; Wang, Y. *Phys. Rev. B* **1992**, *45*, 13244.
(40) Hehre, W. J.; Radom, L.; Schleyer, P. v. R.; Pople, J. A. *Ab initio molecular orbital theory*; Wiley: New York, 1986.
(41) Frisch, A.; Frisch, M. J. *Gaussian 98 User's Reference*; Gaussian, Inc.: Pittsburgh, PA, 1999.
(42) Stephens, P. J. *J. Phys. Chem.* **1985**, *89*, 748.
(43) Bak, K. L.; Jorgensen, P.; Helgaker, T.; Ruud, K.; Jensen, H. J. *J. Chem. Phys.* **1993**, *98*, 8873.
(44) Bour, P.; Keiderling, T. A. *J. Phys. Chem. B* **2005**, *109*, 5348.
(45) Yasui, S. C.; Keiderling, T. A.; Bonora, G. M.; Toniolo, C. *Biopolymers* **1986**, *25*, 79.
(46) Yasui, S. C.; Keiderling, T. A.; Formaggio, F.; Bonora, G. M.; Toniolo, C. *J. Am. Chem. Soc.* **1986**, *108*, 4988.
(47) Yoder, G.; Polese, A.; Silva, R. A. G. D.; Formaggio, F.; Crisma, M.; Broxterman, Q. B.; Kamphuis, J.; Toniolo, C.; Keiderling, T. A. *J. Am. Chem. Soc.* **1997**, *119*, 10278.
(48) Baello, B. I.; Pancoska, P.; Keiderling, T. A. *Anal. Biochem.* **1997**, *250*, 212.
(49) Malon, P.; Kobrinskaya, R.; Keiderling, T. A. *Biopolymers* **1988**, *27*, 733.

(50) Dukor, R. K.; Keiderling, T. A. *Biopolymers* **1991**, *31*, 1747.
(51) Sen, A. C.; Keiderling, T. A. *Biopolymers* **1984**, *23*, 1519.
(52) Yasui, S. C.; Keiderling, T. A. *J. Am. Chem. Soc.* **1986**, *108*, 5576.
(53) Baumruk, V.; Huo, D. F.; Dukor, R. K.; Keiderling, T. A.; Lelievre, D.; Brack, A. *Biopolymers* **1994**, *34*, 1115.
(54) Yoder, G.; Pancoska, P.; Keiderling, T. A. *Biochemistry* **1997**, *36*, 15123.
(55) Martinez, G.; Millhauser, G. *J. Struct. Biol.* **1995**, *114*, 23.
(56) Williams, S.; Causgrove, T. P.; Gilmanshin, R.; Fang, K. S.; Callender, R. H.; Woodruff, W. H.; Dyer, R. B. *Biochemistry* **1996**, *35*, 691.
(57) Decatur, S. M.; Antonic, J. *J. Am. Chem. Soc.* **1999**, *121*, 11914.
(58) Chen, X. G.; Schweitzer-Stenner, R.; Krimm, S.; Mirkin, N. G.; Asher, S. A. *J. Am. Chem. Soc.* **1994**, *116*, 11141.
(59) Manas, E. S.; Getahun, Z.; Wright, W. W.; Degrado, W. F.; Vanderkooi, J. M. *J. Am. Chem. Soc.* **2000**, *122*, 9883.
(60) Bour, P.; Keiderling, T. A. *J. Chem. Phys.* **2003**, *119*, 11253.
(61) Ham, S.; Hahn, S.; Lee, C.; Kim, T.-K.; Kwac, K.; Cho, M. H. *J. Phys. Chem. B* **2004**, *108*, 9333.
(62) Kwac, K.; Cho, M. H. *J. Chem. Phys.* **2003**, *119*, 2247.
(63) Ham, S.; Kim, J. H.; Lee, H.; Cho, M. H. *J. Chem. Phys.* **2003**, *118*, 3491.
(64) Fiori, W. R.; Miick, S. M.; Millhauser, G. M. *Biochemistry* **1993**, *32*, 11957.
(65) Tirado-Rives, J.; Maxwell, D. S.; Jorgensen, W. L. *J. Am. Chem. Soc.* **1993**, *115*, 11590.
(66) Zhang, L.; Hermans, J. *J. Am. Chem. Soc.* **1994**, *116*, 11915.
(67) Smythe, M. L.; Nakaie, C. R.; Marshall, G. R. *J. Am. Chem. Soc.* **1995**, *117*, 10555.
(68) Young, W. S.; Brooks, C. L., III *J. Mol. Biol.* **1996**, *259*, 560.
(69) Ham, S.; Choi, J.-H.; Cho, M. H. *J. Chem. Phys.* **2003**, *119*, 1451.
(70) Woutersen, S.; Hamm, P. *J. Phys. Chem. B* **2000**, *104*, 11316.
(71) Woutersen, S.; Hamm, P. *J. Chem. Phys.* **2001**, *115*, 7737.
(72) Schweitzer-Stenner, R. *Biophys. J.* **2002**, *83*, 523.
(73) Yasui, S. C.; Keiderling, T. A.; Katachai, R. *Biopolymers* **1987**, *26*, 1407.
(74) Yasui, S. C.; Keiderling, T. A. *Biopolymers* **1986**, *25*, 5.
(75) Singh, R. D.; Keiderling, T. A. *Biopolymers* **1981**, *20*, 237.
(76) Hol, W. G. J. *Prog. Biophys. Mol. Biol.* **1985**, *45*, 149.
(77) Lockhart, D. J.; Kim, P. S. *Science* **1992**, *257*, 947.